Oxidation effects on spark plasma sintering of molybdenum nanopowders

Geuntak Lee, Christina Back, Eugene A. Olevsky, Charles Manière, Joanna Mckittrick, Anthony Gattuso, Eugene A Olevsky

Oxidation effects on spark plasma sintering of molybdenum nanopowders

Geuntak Lee

Charles Manière

Joanna McKittrick

Anthony Gattuso

Christina Back

Eugene A. Olevsky

Abstract

Surface-oxidized molybdenum nanopowders are compacted by spark plasma sintering (SPS). The oxide impurity behavior is analyzed under various sintering temperatures. The densification mechanism of the nanopowders with a melted oxide phase is identified in situ by regression analysis of the experimental data on the temperature-dependent porosity change and on the SPS multistep pressure dilatometry. To increase the density of the compacted pellets, the nanopowders with the oxide phase are consolidated by SPS using the two in situ oxide removal methods: carbothermic reduction and particle surface cleaning by the electric current flow through the powders. The advantages and disadvantages of these methods in terms of the density, grain size, and mechanical properties of the final products are discussed.

1 INTRODUCTION

Molybdenum (Mo) powder-based components are used for many industrial applications due to favorable physical, chemical, and mechanical properties, such as high melting temperature (2623°C), high corrosion resistance and weldability, low thermal expansion coefficient, and high thermal conductivity.1-3 However, Mo products with large porosity and coarse grain structure exhibit poor mechanical strength. Therefore, studies to produce dense Mo products with small grain size are in great demand.

A significant challenge in sintering of metal powders is the presence of a natural oxide layer at the surface of particles. In particular, metal nanopowders, which have higher surface area and energy, are easily oxidized compared to micron-sized powders. Particularly, Mo nanopowders generally show the pyrophoric behavior when exposed to an air, so special care is required to avoid the possible formation of a surface oxide during powder handling and storage.4

The surface oxide layer in the powders hampers the mass transports and impedes the diffusion between the powder particles.5 Munir et al6 studied the role played by surface oxide layers in the kinetics of sintering of metal particles, and showed that the onset of sintering was delayed by the presence of the surface oxide phase. Specifically, the palladium particles with surface oxide layers modified the sintering mechanism from the grain-boundary diffusion to the surface diffusion below the oxide dissociation

temperature. After the dissociation of the oxide, the mechanism of the sintering of palladium converts back to the grain-boundary diffusion.7

The creep parameters of Mo with micron-scale grain size were studied extensively.8-10 Creep exponent (n) was determined to be approximately 4.85, indicating the dislocation creep controlled by the dislocation climb mechanism, generally observed in most polycrystalline metals.11 The creep test under 1500°C-1600°C and 62 MPa indicated the n value of 4.5 with an activation energy (Q) of 480 kJ/mol, which was slightly higher than the activation energy for lattice diffusion (405 kJ/mol).12 Also, Carvalhinhos et al13 based on the compression and tension tests, showed the n value to be in the range of 5.2-5.8 with Q value being in the range of 257-369 kJ/mol. However, the creep parameters for nano-grained Mo at elevated temperatures (~0.5Tm) cannot be directly experimentally found due to the grain growth during the creep test. By the aid from the grain growth inhibitor like ZrC particles located at the grain boundaries, the creep of the Mo alloy with 0.8 mol% dispersed zirconium carbide (ZrC) and with the 300 nm average grain size under 1500°C indicated the superplasticity behavior (n = 2.44).1, 2, 14 At near ambient temperature, the nanoindentation creep data of Mo thin film (30-40 nm grain size) showed that the creep exponent was close to 6.67—the value related to the thermally activated glide-controlled creep.15, 16

The phase diagram of Mo–O by Phillips and Chang17 shows that about four stable oxides exist below the temperature around 820°C: MoO_2, MoO_3, and two intermediate phases Mo_4O_{11} and Mo_9O_{26} in composition.18 MoO_2 melts around 2327°C.18 Otherwise other oxide phases like MoO_3, Mo_4O_{11}, and Mo_9O_{26} can be melted around 820°C and can be vaporized near 1300°C.18, 19

It should be noted that the research on oxide effects on the densification mechanisms of Mo nanopowders at high temperatures was limited. With the micron-sized Mo powders, Lee et al20 studied the influence of the oxygen concentration on the Mo grain size and hardness of pellets compacted by spark plasma sintering (SPS). Mo powders with reduced oxygen content were obtained by solid-state reduction method using metallic calcium as a deoxidizer. It was shown that, compared to the samples with a high oxygen content, samples with lower oxygen content had larger hardness values due to the higher density and smaller grain size enabled by the reduction in oxide impurities at the Mo grain boundaries. It was reported that the impurity level of the oxygen can distort the atomic structure near the grain boundaries and therefore facilitate defect or Mo diffusion.21 However, the in situ removal of the surface oxide layer during sintering should provide great benefit to the production of small grain sized, dense Mo parts.

Some in situ oxide removal methods have been tried for the sintering of metal powders. First, the sintering under hydrogen atmosphere can be performed to reduce the oxide. Majumdar et al22 removed the oxide phase by holding Mo powders specimens at 900°C for 15 minutes in the presence of H_2 gas during the conventional oven sintering. However, the in situ oxide reduction during sintering, if possible without using the flammable hydrogen gas, is highly desirable considering the time and safety. Second, the oxide coating of metal powders can be removed by the addition of the carbon powders to starting powders, which results in the reaction of carbon and oxide (carbothermic reaction). This method has been used to remove the surface oxide during the pressure-assisted or pressure-less sintering of SiC,23-

25 B4C,26, 27 and ZrB2.28 Since the oxide is removed via the gas phase, the gas diffusion is the rate-limiting step for the complete removal of the oxide phase.26 Third, during SPS, surface cleaning from the presence of high-temperature plasma between particles can be used for an in situ oxide removal.29, 30 Groza et al29 stated that in addition to conventional plasma, the plasma during SPS can be non-conventional; local and transient plasma can be dissipated by expanding through the gas spaces and recombining at the adjacent material particle surfaces. Kim et al31 claimed that the oxide phase is removed by holding the temperature at 1300°C for 1 hour in the middle of the SPS process for B4C sintering. However, the existence of the plasma is still controversial in SPS setup.32-36 The second and the third above-mentioned methods have not been applied to the sintering of Mo nanopowders.

In the present study, the effect of oxygen on the densification kinetics of Mo nanopowders was investigated using in situ methods37: carbothermic reduction and particle surface cleaning. The efficiencies of each oxide reduction method are compared. The sintering constitutive parameters based on the regression analysis of the experimental data on the porosity evolution using the continuum theory of sintering were determined.38-40 The effect of the oxygen content on the density and mechanical properties of the sintered samples are also discussed.

2 METHODS

2.1 In situ determination of sintering constitutive parameters

Each of the densification mechanisms for a powder material high-temperature creep has specific values of the creep exponent (n) and creep activation energy (Q), by which these mechanisms can be defined uniquely.11, 41 A direct in situ method based on the continuum theory of sintering is used here to identify the sintering mechanism for Mo nanopowders.

Initially, the regression analysis renders the temperature-dependent creep parameters (A0 [pre-exponential constant of power-law creep equation (K/(s Pan)], Q (kJ/mol) and n) based on the SPS experiment at the ramping temperature and assuming the traditionally used expressions of the normalized shear and bulk moduli.38 When n value cannot be unambiguously determined from the regression analysis, the SPS multistep pressure approach is used.40 The detailed derivation of the sintering parameters can be found elsewhere.37, 38

The linearization of the constitutive equation of the pressure-assisted sintering39 can be expressed as follows:

$$n \ln\left(\frac{|\sigma_z|}{\left(\psi+\frac{2}{3}\phi\right)^{n+1/2n}(1-\theta)^{n-1/2n}|\dot{\varepsilon}_z|^{1/n}}\right)-\ln(T)=-\ln(A_0)+\frac{Q}{RT} \quad (1)$$

where φ is the normalized shear modulus, ψ is the normalized bulk modulus, $|\sigma_z|$ is the applied axial stress (Pa), $|\dot{\varepsilon}_z|$ is the strain rate of the sample (s^{-1}), θ is the porosity, T is the temperature (K), and R is the gas constant (J/mol K).

For each *n* value, various theoretical porosity evolution curves can be plotted using the obtained creep parameters (A_0, Q) based on the constitutive equation of sintering assuming the same experimental sintering conditions (T and $|\sigma_z|$),**39** and these curves can be compared with the experimental porosity evolution data. However, in many cases, when using this method, the determination of the parameter *n* value is difficult due to the low accuracy**37**; therefore the SPS multistep pressure dilatometry approach is a more reliable approach to utilize.

For the SPS multistep pressure dilatometry40 approach, the *n* value can be determined by the following equation:

$$n = \frac{\ln\left(\frac{\exp(-|\epsilon_{z2}|)-(1-\theta_0)}{\exp(-|\epsilon_{z1}|)-(1-\theta_0)}\frac{|\dot{\epsilon}_{z1}|}{|\dot{\epsilon}_{z2}|}\right)}{\ln\left(\frac{\sigma_{z1}}{\sigma_{z2}}\exp(|\epsilon_{z2}|-|\epsilon_{z1}|)\sqrt{\frac{\exp(-|\epsilon_{z2}|)-(1-\theta_0)}{\exp(-|\epsilon_{z1}|)-(1-\theta_0)}}\right)} \quad (2)$$

where indices 1 and 2 indicate the different compressive strain $|\epsilon_z|$ and strain rates $|\dot{\epsilon}_z|$ and stress σ_z before and after the pressure jump, and ϑ_0 is initial porosity prior to each pressure jump.

Using the above-mentioned approach, the creep parameters (A0, Q, and n) can be obtained via only one or two (when SPS multistep pressure dilatometry is not required or required, respectively) experiments.

2.2 In situ oxide removal strategies

Two strategies were employed to remove the oxide during sintering of Mo nanopowders with the natural oxide layer at the surface.

In the first strategy, the reaction of Mo oxide with carbon powders was employed during SPS process (Figure 1A). The carbothermic reduction in the nano-sized MoO3 phase to the Mo phase was studied by Saghifi et al.42, 43 Using differential temperature analysis and temperature gravimetric analyses (DTA/TGA), the following reactions were suggested:

$$2MoO_3 + C = 2MoO_2 + CO_2,\ \Delta G(298\,K) = -122.3\,kJ/mol \quad (3)$$

$$MoO_2 + C = Mo + CO_2,\ \Delta G(298\,K) = 130\,kJ/mol \quad (4)$$

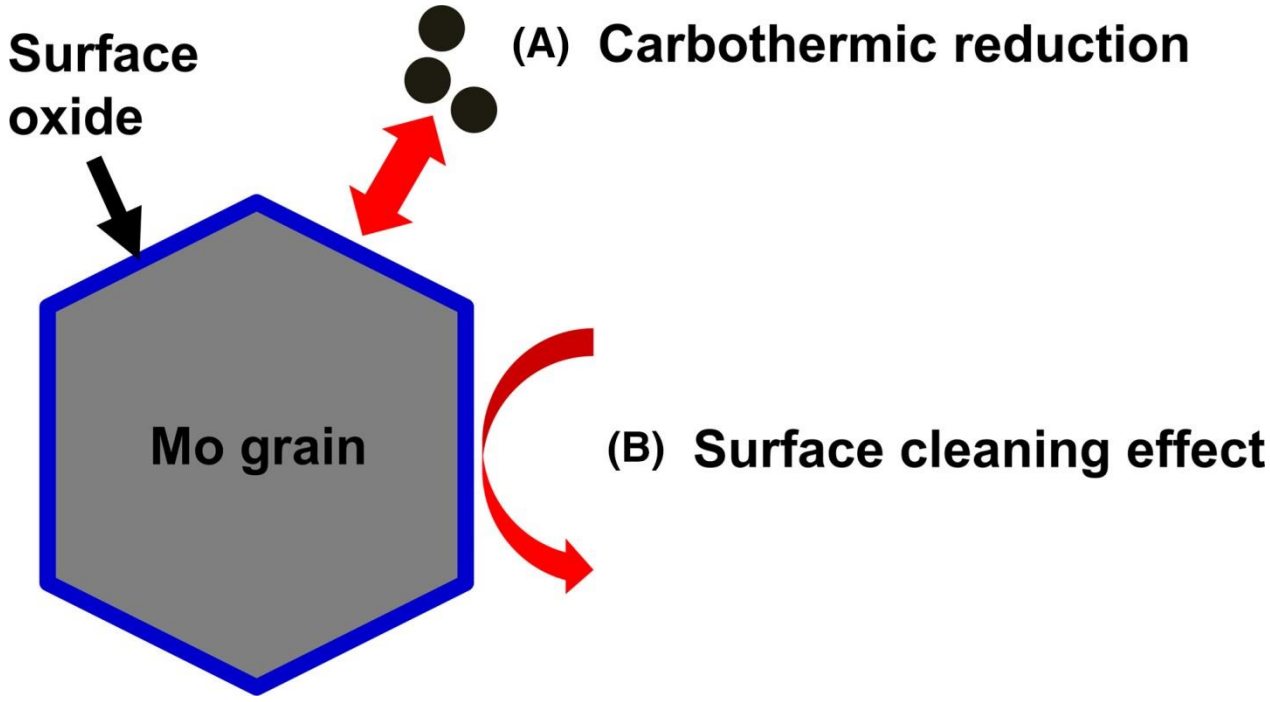

F1 In situ oxide reduction strategies during sintering. A, carbothermic reduction and B, surface cleaning effect

Based on this analysis, Saghifi et al42, 43 showed two steps for the carbothermic reduction in MoO3 to Mo. First, MoO3 is heated to 600°C with holding for 1 hour for the complete reduction in MoO3 to MoO2. Next, the heat treatment at 1000°C for 1 hour provides the reduction in MoO2 to Mo.

In the present study, the similar steps were applied during Mo nanopowders' compaction by SPS. The carbothermic reduction produces the CO or CO2 gas. Since the gas diffusion is a critical factor for the densification,26 the low uniaxial pressure of about 15 MPa was used for easy outgassing at the initial and intermediate stages of sintering in the SPS vacuum chamber. At the end of the carbothermic reduction, the pressure has been increased to 60 MPa to enhance the densification of Mo nanopowders.

For the second strategy, the oxide phase can be removed by the electric current flow through the Mo particles during SPS, using the surface cleaning effect (Figure 1B). The high-energy electric field generated by the high electric current removes the oxide layer.29, 30 During the initial stage of SPS, the small amount of the electric current can flow into the Mo powders through the neck generated from the removal of the oxide layer either by the dielectric breakdown or by the applied pressure.44-46 By increasing temperature and the corresponding electric current during SPS, the induced plasma removes the oxide layer which results in the intensified neck formation between the particles. Therefore, more electric current flows through the Mo powders, and the surface cleaning effect is expected to be strengthened with the sintering temperature and time. In this study, to form many necks during the initial stage of the sintering and to render a more pronounced electric current induced surface cleaning effect, the 60 MPa pressure was applied to mechanically break the oxide layer at the particle surface

before the start of SPS and was maintained during the whole SPS duration. The 800°C used for the soaking stage is the temperature before the onset of the sintering of Mo (Section 4.4).

3 EXPERIMENTAL PROCEDURES

The commercial Mo nanopowders (US Research Nanomaterials, Houston, USA) with a labeled purity of 99.9% (metal basis) and Carbon Black nanopowders (MTI Corporation, Richmond, VA) were used for this research.

The sintering process was carried out using the SPS system (Dr. Sinter SPSS-515; Syntex, Kanagawa, Japan) with a tooling setup made from the EDM4 graphite (Poco Graphite, Decatur, TX). A 0.15 mm-thick graphite paper wrapped the powder to prevent adhesion between the specimen and the tooling. An optical pyrometer (IR-AHS2; Chino, Tokyo, Japan) was used to detect the temperature (Tdie) at the 2.5 mm depth hole in the graphite die.

SPS conditions to investigate the consolidation behavior of the surface-oxidized Mo nanopowders included the heating rate of 100°C/min from 600°C to the maximum temperature (1100, 1200, 1300, 1600, or 1700°C) with 60 MPa applied pressure and no holding time under vacuum. The control experiments to get the thermal expansion of the graphite die set were carried out under the same SPS conditions without Mo nanopowders.

Finding the densification mechanism requires the exact measurement of the Mo powders temperature during SPS. The temperature of the Mo nanopowders (Tsample) during SPS compaction was measured by inserting a k-type thermocouple directly into the Mo nanopowder. For the regression analysis, the SPS data obtained from the compaction of the Mo nanopowder with a maximum die temperature of 1300°C (Tsample = 1391°C) were used. For the SPS multistep pressure dilatometry approach, with 100°C/min and the minimum pressure under vacuum, the surface oxidized Mo nanopowders were heated up to 950°C (Tsample = 992°C), which exceeds the melting point of the Mo oxide phases except the MoO_2 phase. After stabilization of the temperature during the holding stage, a few successive jumps of the pressure were applied to measure the variation in the strain rate at each pressure jump. Except for the experiments for regression analysis (Section 4.4), the temperature described in this study refers to "Tdie".

For preparing the carbothermic reduction (Figure 1A), the Mo nanopowders were mixed with carbon nanopowders in the cyclohexane by ultrasonication for 30 minutes. Mo + C nanocomposite suspension was frozen by liquid nitrogen for 10 minutes and subjected to freeze-drying (Freezone 1; Labconco, Kansas City, MO) at −50°C for 24 hours. For the in situ carbothermic reduction during SPS, the following steps were used in Ar atmosphere: (a) ramping to 600°C with 17 MPa pressure, (b) holding at 600°C for 15 minutes, (c) ramping to 1000°C with 100°C/min, (d) holding at 1000°C for 30 minutes and increasing pressure to 60 MPa during the last 2 minutes of the holding stage, (e) ramping to 1300°C with 100°C/min, and (g) holding at 1300°C for 10 minutes. For comparison, an SPS test was conducted under the same conditions without the addition of carbon to the Mo powders.

To employ the second strategy (Figure 1B), the powders were heated to 800°C under 60 MPa pressure and soaked for 30 minutes, and then heated to the final sintering temperatures of 1200°C or 1700°C with 100°C/min and 0 or 10 minutes holding time using Ar atmosphere during SPS. For comparison, an SPS test was conducted under the same conditions without the soaking stage at 800°C.

The theoretical densities of Mo and carbon nanopowders were measured by the pycnometer (AccuPyc 1330; Micromeritics Instrument, Norcross, GA). The densities of the sintered Mo specimens were measured by the Archimedes method. The particle (or grain) size and composition were assessed by the scanning electron microscopy (FEI Quanta 450; Thermo Fisher Scientific, Waltham, MA) and energy-dispersive X-ray spectroscopy (EDS; Oxford Instruments, Abingdon, UK). The compositions of the powders and Mo pellets were obtained by the average of six measurements by EDS. It should be noted that the compositions determined by EDS have limited value in the quantitative analysis due to the interaction volume associated with the method. Hence, the determination of species that may segregate to surfaces (eg, surface oxide impurities such as Mo oxide phase in this study) is problematic because much of the chemical information comes from the bulk of the specimen. Due to this limitation, EDS was used only as a comparative tool for this study. The well-polished specimens were etched with Murakami's reagent (Solution of 200 mL DI water, 10 g KOH and 10 g K3[Fe(CN)6] for 30 seconds. The transverse rupture strength (TRS) of the compacted Mo pellets was measured. The experimental method to measure the TRS can be found elsewhere.47

4 RESULTS AND DISCUSSION

4.1 Powder characterization

As shown in Figure 2A,B, Mo nanopowders particles have a round shape and are agglomerated. By the particle size analysis, the Mo nanopowders showed a broad size distribution from 50 nm to 2 μm with an average particle size of 200 nm. The micron-sized Mo particles (non-agglomerated) are indicated as red arrows shown in Figure 2B. X-ray diffraction (XRD) analysis in previous study48 showed that Mo nanopowders have large Mo peaks and small Mo oxide peaks. Also, 27.3 at.% of oxygen contents were detected on the surface of Mo nanopowders by EDS measurement. The theoretical density of Mo is 10.2 g/cm.3 The density measurement of the Mo nanopowders by the pycnometer showed 9.68 g/cm3 possibly due to the lower theoretical density of Mo oxide phases such as MoO_2 (6.47 g/cm³) and MoO_3 (4.69 g/cm³). Therefore, we assumed that Mo nanopowders are highly oxidized and have the form of Mo core with Mo oxide layer at the surface. The carbon nanopowders have an average particle size of 50 nm and show agglomeration (Figure 2C).

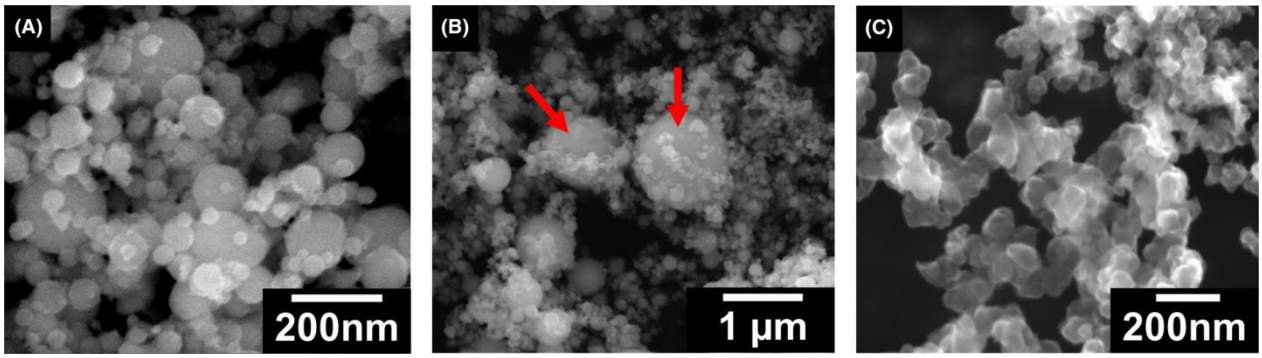

F2 SEM image A, 120 000× and B, 25 000× for Mo powders, and C, 100 000× for carbon powders. Red arrows indicate large Mo particles

4.2 Surface oxidized Mo nanopowders consolidated by spark plasma sintering

Figure 3 displays the SEM images of Mo pellets compacted by SPS at different temperatures under the same conditions of 60 MPa, 100°C/min, 0 minute holding time and vacuum. Using EDS analysis, it was revealed that the black regions correspond to the Mo oxide phase (solid arrow with red) or pores (short-dashed arrow with green), and white regions were Mo in the SEM phase images (Figure 3A-C). Also, EDS showed that the ripped debris (blue circle in Figure 3D) between the Mo grains of the fractured pellets are the Mo oxide phase. As shown in Figure 3A, the melted oxide and pores were distributed between the Mo nanopowders (white color), and some Mo particles are connected by necks. At 1300°C, the neck areas between Mo particles are increased and the average grain size is increased up to about 2 µm (Figure 3B). After the neck area increases, the grain size increases rapidly with increasing the sintering temperature but without densification which will be discussed later (Figures 3B-D).

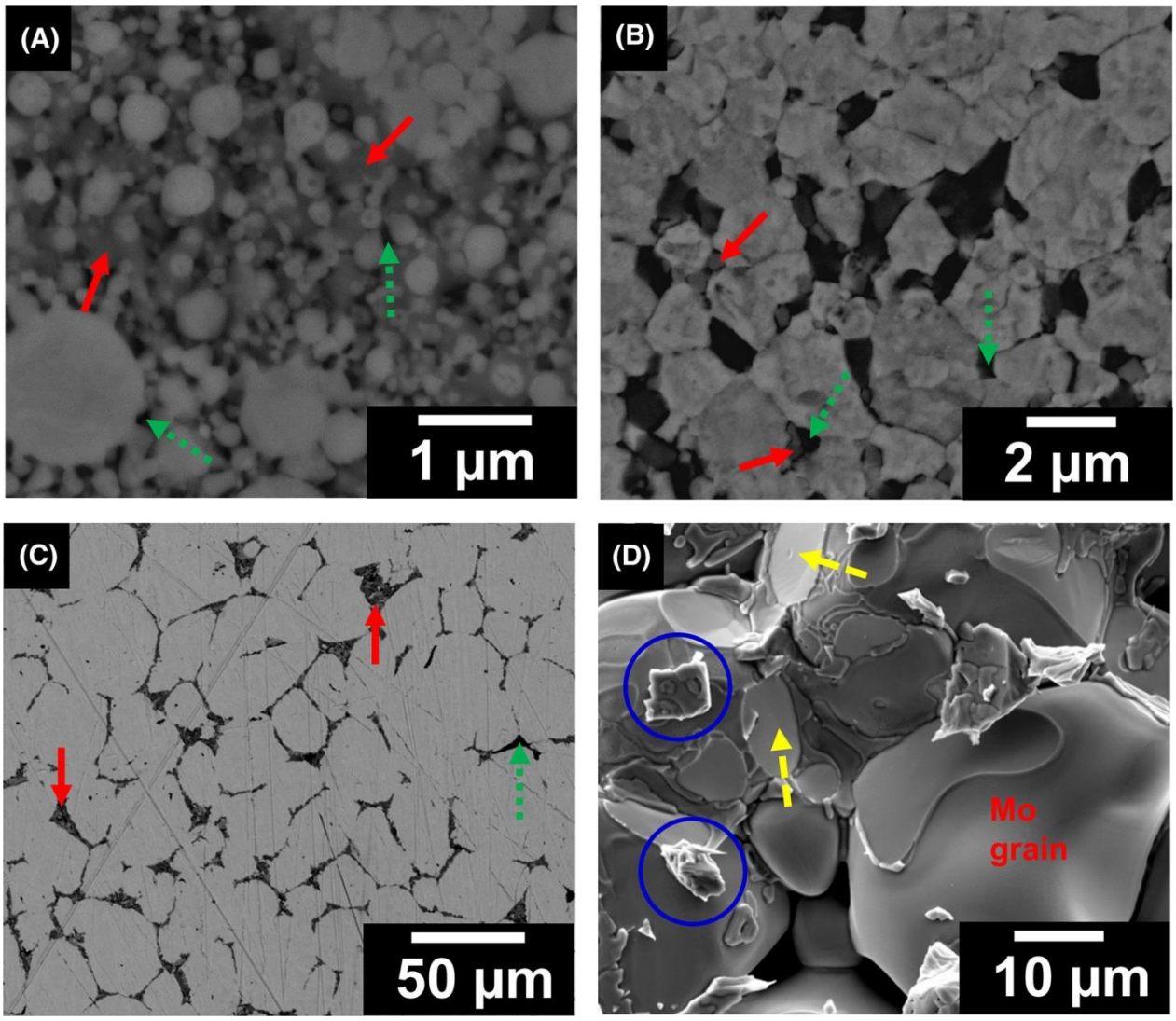

F3 SEM image of Mo pellets densified at A, 1100°C, B, 1300°C and C, 1600°C and D, 1700°C, respectively. The solid red, short-dashed green and long-dashed yellow arrows indicate the representative Mo oxide phase, pore, and neck, respectively. The blue circle indicates the ripped Mo oxide debris from the fractured Mo pellets

The behavior of the surface oxide is schematically shown in Figure 4. The densification map indicating the density, TRS, grain size, and oxygen content is shown in Figure 5. At the low temperature, the neck formation between Mo powders is mostly inhibited by the liquid film of the oxide, resulting in the retardation of the onset of the sintering and the grain growth49 (Figure 4A). After melting of the surface oxide layer, the molten oxide moves to the porous regions between the Mo particles. Some pores are partially filled with the oxide phase (Figure 3A and 4B). Similarly to the Ostwald ripening during liquid phase sintering,50 the densification induced by the grain growth can be observed at this stage through the dissolution and precipitation of atoms (solution-reprecipitation).51 However, there is no significant grain growth during the densification as shown in Figure 5. Therefore, the solution-reprecipitation is not the dominant mass transport mechanism in this study.

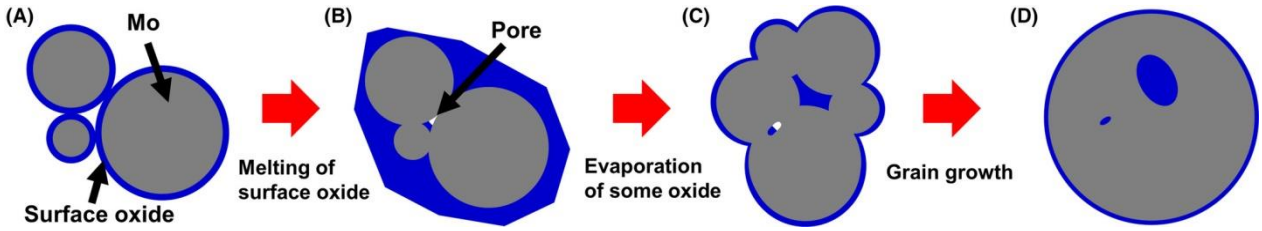

F4 Schematics of the behavior of the surface oxide during SPS of Mo nanopowders

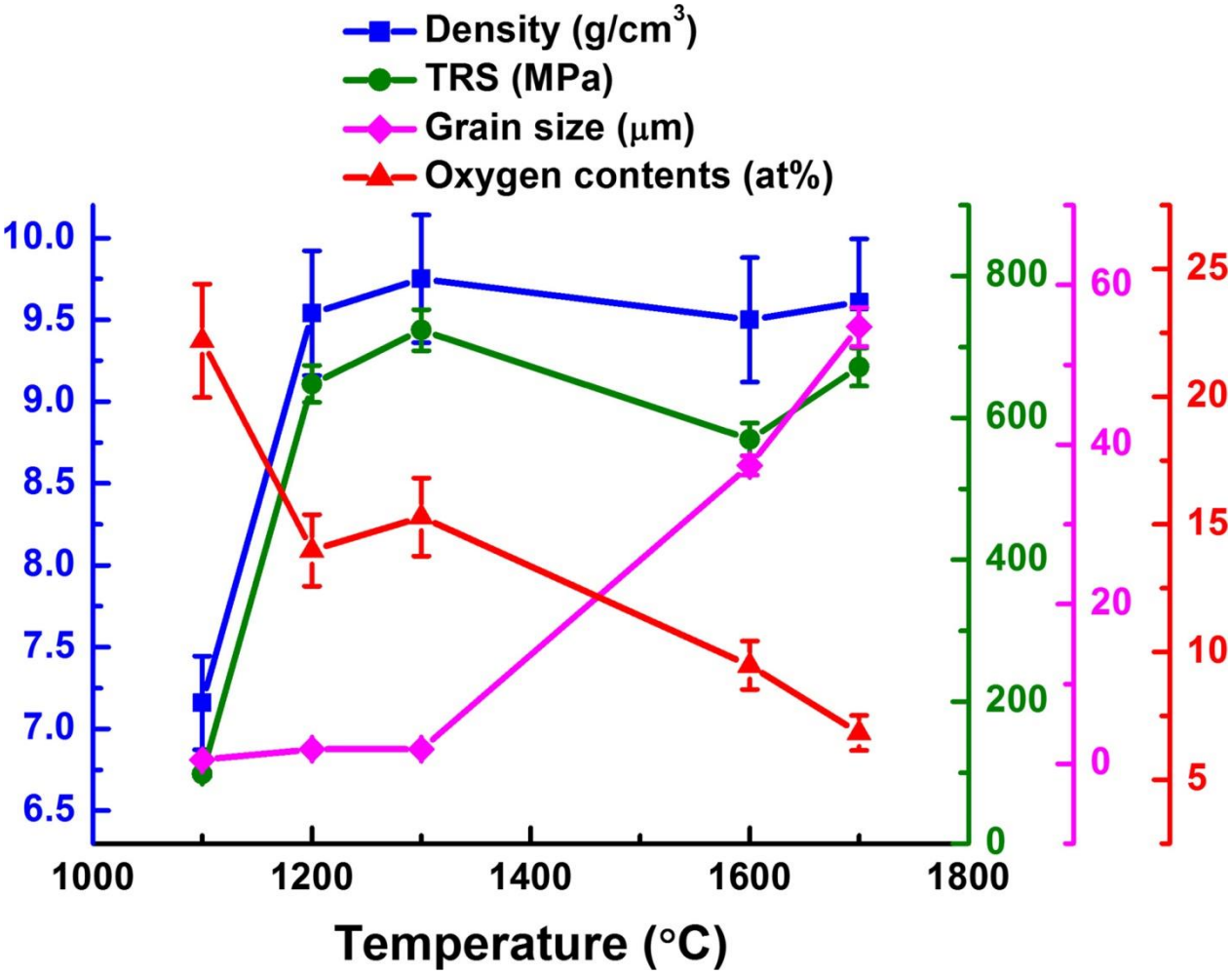

F5 The density, TRS, grain size, and oxygen content change with sintering temperature 1100°C, 1200°C, 1300°C, 1600°C, and 1700°C in SPS with 60 MPa, no holding time and vacuum

With increasing temperature, most of the oxides are evaporated and diffuse out to the chamber through the open porous path, but some oxides remain due to a block of the gas diffusion path by the densification. Also, the MoO2 phase can be remained due to the high melting point.

Due to evaporation, the amount of the oxide in the samples is reduced, and then the neck area between the Mo particles increased, simultaneously resulting in the grain growth. Some oxide is trapped in the grains during the coalescence of the grains (Figures 3C,D and 4C,D). With an increase in the sintering

temperature, the grains become larger and then the melted, non-melted or evaporated oxide occupy the grain-boundary regions and can recrystallize during the cooling stage (red solid arrows and blue circles in Figures 3C,D).

The surface oxides have two effects on the sintering behavior, depending on the quantity. First, large amounts of the oxide phases which is sufficient to surround the Mo grains, can act as a physical obstacle to contact between the Mo grains, resulting in a delay of the neck formation, the onset of densification and the grain growth when the solution-reprecipitation by liquid phase is limited.6, 51 Otherwise, small amounts of oxide near the grain-boundary regions can affect the grain growth behaviour.21 It is reported that the impurity or dopant level (0.1-1 at.%) of the atoms can distort the atomic structure near the grain boundaries and therefore facilitate the defect migration.52, 53 Therefore, Mo grains with nearby dopant level of an oxide can grow faster than those of pure Mo.

The oxygen content decreased with increasing sintering temperature due to the evaporation of some oxide phase, which induced the rise of the density at temperatures < 1300°C, as shown in Figure 5. Most of the open pores, which provide the fast diffusion path for the gas, have been closed due to the increase in the density at temperature < 1300°C.

After closing the open pores, the following phenomena affect the overall change in the pellet density:

Densification via

1. The Mo atom diffusion and interface reaction through the oxide at the grain boundaries;

2. The evaporation of Mo oxide (Mo oxide has lower theoretical density compared to that of pure Mo).

Swelling via

1. The pore creation by the removal of Mo oxide;

2. The carbon diffusion into the edge of the samples from the graphite paper and the die during SPS35, 54 (Mo carbide has lower theoretical density compared to that of pure Mo).

Therefore, the density of the pellets increases or decreases due to the mutual compensation of the densification and swelling effects.

Tensile rupture strength is dependent on the porosity and grain size of the materials. However, TRS shows a greater dependence on the porosity of Mo pellets rather than on the grain size in this study (Figure 5). The porous regions of the Mo pellet are filled with the melted oxide which promotes the embrittlement, and the presence of the oxide phase dominates the overall mechanical behavior of the Mo pellets.

As analyzed before, the surface oxide limits the densification and increases the grain size enormously during the Mo nanopowder sintering. Therefore, in order to increase the density of the Mo pellets, various in situ oxide reduction methods have been employed, as described in section 4.5 and 5.

4.3 Densification mechanism of oxidized Mo nanopowders

There is 4.5% increase in density mainly due to the nanopowders rearrangement by the pressure, and pore filling by the melted oxide before the onset of sintering around 900°C (Tsample; Figure 6A). However, an abrupt increase in the density due to liquid phase formation was not observed in this study like during regular liquid phase sintering. During the ramping stage of SPS, the temperature distribution of the Mo pellet can be non-homogeneous, which affects the region of melting of the oxides.55 The SPS device records the Z-displacement corresponding to the slowest densification rate, therefore fast densification by particle rearrangement within the liquid phase cannot be detected. Also, the different forms of the Mo oxides have the different melting temperatures, which affect the Z-displacement behavior in SPS.19

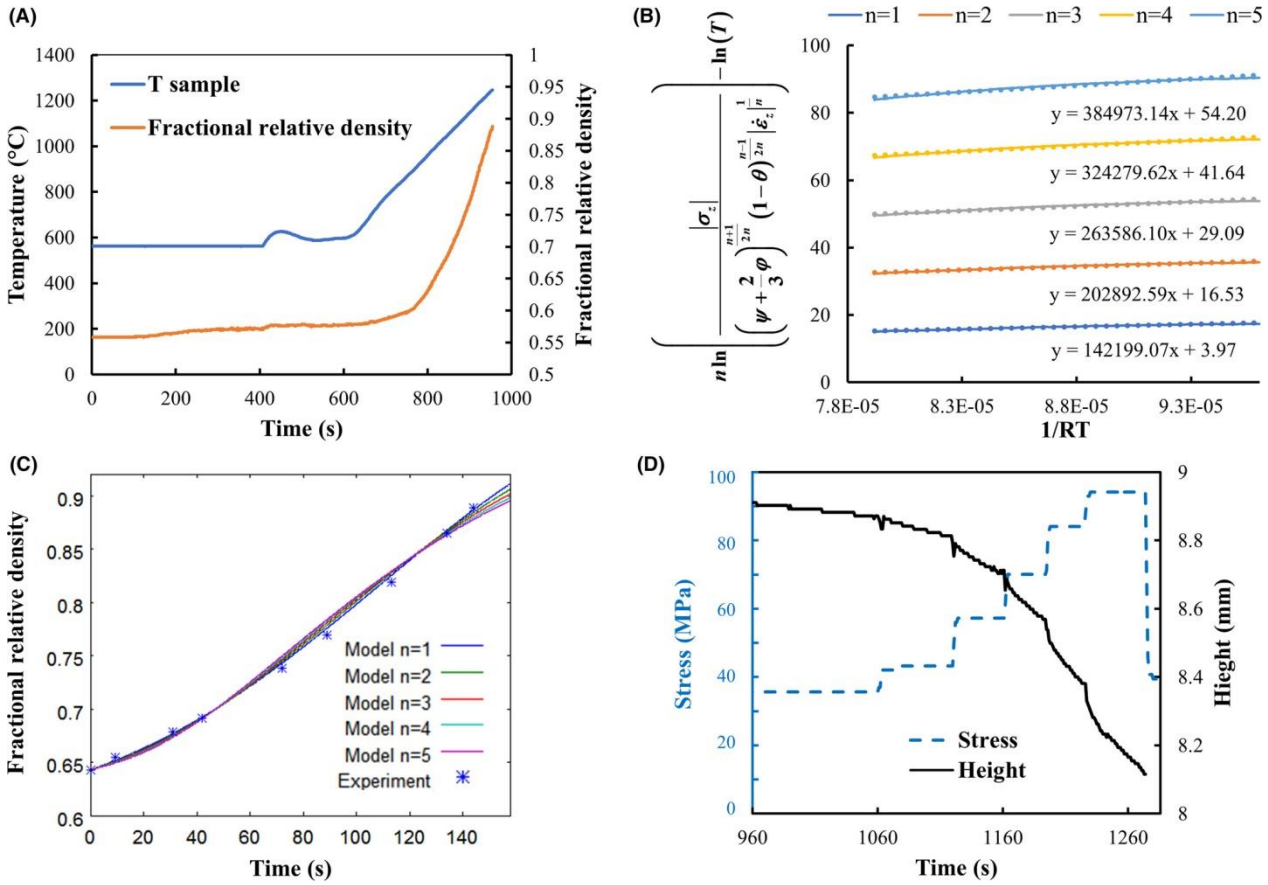

F6 The steps to find the sintering mechanism of surface-oxidized Mo nanopowders compacted by SPS. A, Experimental SPS results: temperature (Tsample) and fractional relative density. B, Linearization curves for each n values (the fitting equations are shown on the bottom of each curve). C, Modeled/experimental fractional relative density curves using identified parameters from regression approach for each tested n values. D, Change in applied stress and height of sample during isothermal stage in multistep pressure method

After melting of some oxides, the particles become connected, forming necks and starting densification > 900°C (Tsample). The experimental SPS densification data (Figure 6A) were used to plot the linearized

densification curves for different n values (1-5) using Eq. 1, as shown in Figure 6B. The fractional relative density ranges from 0.64 to 0.89 are used from Figure 6A to exclude the effect of the grain growth on the sintering kinetics. The fitting equations for each n value are shown at the bottom for each curve in Figure 6B. Parameter A0 and Q values for each n, using Equation 1, are listed in Table 1.

Table 1. Creep parameters identified from regression approach of the porosity evolution curve in Figure 6A

n	**1**	**2**	**3**	**4**	**5**
Q (kJ/mol)	142.20	202.89	263.59	324.28	384.97
A_0 (K/(s Pa^n))	1.881E-2	6.624E-8	2.334E-13	8.224E-19	2.898E-24

Figure 6C shows the modeled/experimental fractional relative density curves using the identified sintering parameters through the regression analysis of the constitutive parameters for each of the tested n values (Table 1). However, the comparison of the experimental and theoretical density curves doesn't indicate a unique n value, as shown in Figure 6C, therefore the complementary SPS multistep pressure dilatometry was used to find the distinctive n value. Figure 6D shows the change in the stress and height of a sample during the multistep SPS of the surface-oxidized Mo nanopowders for the isothermal SPS stage under 950°C (Tsample = 992°C). When there is a jump of the pressure, the slope of the sample height is altered accordingly indicating the change in the strain rate for each jump. From the data in Figure 6D, the average n value estimated using Equation 2 is 4.86. With this average n value, one can expect the value of parameter Q to be in the range from 324 kJ/mol (n = 4) to 385 kJ/mol (n = 5), as shown in the Table 1 in terms of the regression-based data.

The obtained n and Q values from this study indicate that the sintering mechanism of the surface-oxidized Mo nanopowders after melting of the Mo oxide phase is dislocation creep controlled by dislocation climb, which is the same mechanism (n = 4.85-5) identified based on the creep test of Mo with a grain size of 150 µm.10 The dislocation climb mechanism requires lattice diffusion,11 and indeed, the effective activation energy obtained (324.28-384.97 kJ/mol) is more close to the reported Ql value (activation energy for the lattice diffusion) of 405 kJ/mol compared to Qgb value (activation energy for the grain-boundary diffusion) of 263 kJ/mol.10 The obtained lower activation energy compared to Ql can be caused by the increasing role of the grain-boundary diffusion due to the smaller size of Mo powder particles used in this study compared to conventional micron-sized Mo powders.

Prior to the melting of the oxide, the diffusion of Mo atoms is limited and only can be possible via the surface diffusion mechanism due to the existence of the surface discontinuity in the surface layer caused by the compaction pressure,7 Mo precipitation from Mo oxide, or via Mo diffusion through Mo oxide from other particles. After melting of the oxide layer, inter-particle necks are formed. Since the bridges

for the dislocation movement are formed, dislocation creep may be the most probable sintering mechanism in this temperature range (about 0.4Tm) and pressure (60 MPa): Diffusional creep (n = 1) requires high temperature about 0.9Tm. Grain-boundary sliding (n = 2), which is often observed during the creep of nanograined materials, is restricted in this case due to the presence of the oxide phase between the grains. When the oxide is removed, diffusion through the grain boundary has a critical role due to the large grain-boundary area of Mo nanopowders. Indeed, our ongoing studies show that the densification mechanism of Mo nanopowders without surface oxide is the grain-boundary sliding controlled by the grain-boundary diffusion at the same temperature range (of about 0.4Tm).

4.4 Carbothermal reduction in oxidized Mo nanopowders during SPS

Mo with a different amount of added carbon was densified by SPS under the same conditions (1300°C, 60 MPa, 100°C/min and 10 minutes holding time, Ar gas). Figures 7A-C show the SEM images of the obtained samples with different additions of carbon. The corresponding XRD pattern from the samples is shown in Figure 7D. Figure 8 shows the effect of the carbon addition on the density, TRS, oxygen contents, and carbon contents of the Mo pellets compacted by SPS.

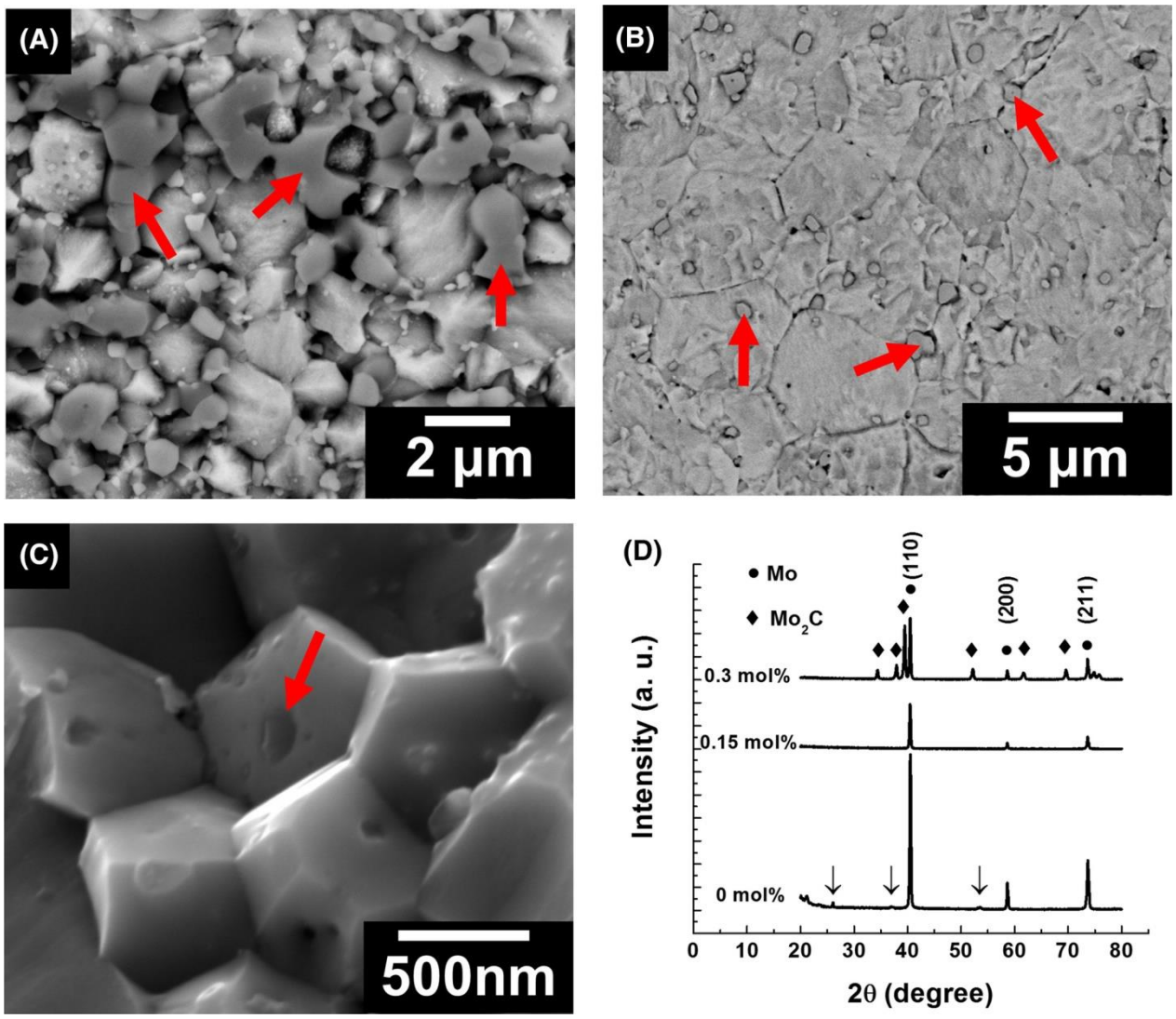

F7 SEM images of SPSed Mo pellets consolidated with different carbon contents: A, No carbon added. B, 0.15 mol% and C, 0.3 mol% carbon added. Red arrows indicate the Mo oxide phase. D, XRD of compacted Mo pellets. The circle and diamond symbols indicate Mo and Mo2C phases, respectively. Black arrows indicate the peaks corresponding to the MoO2 phase

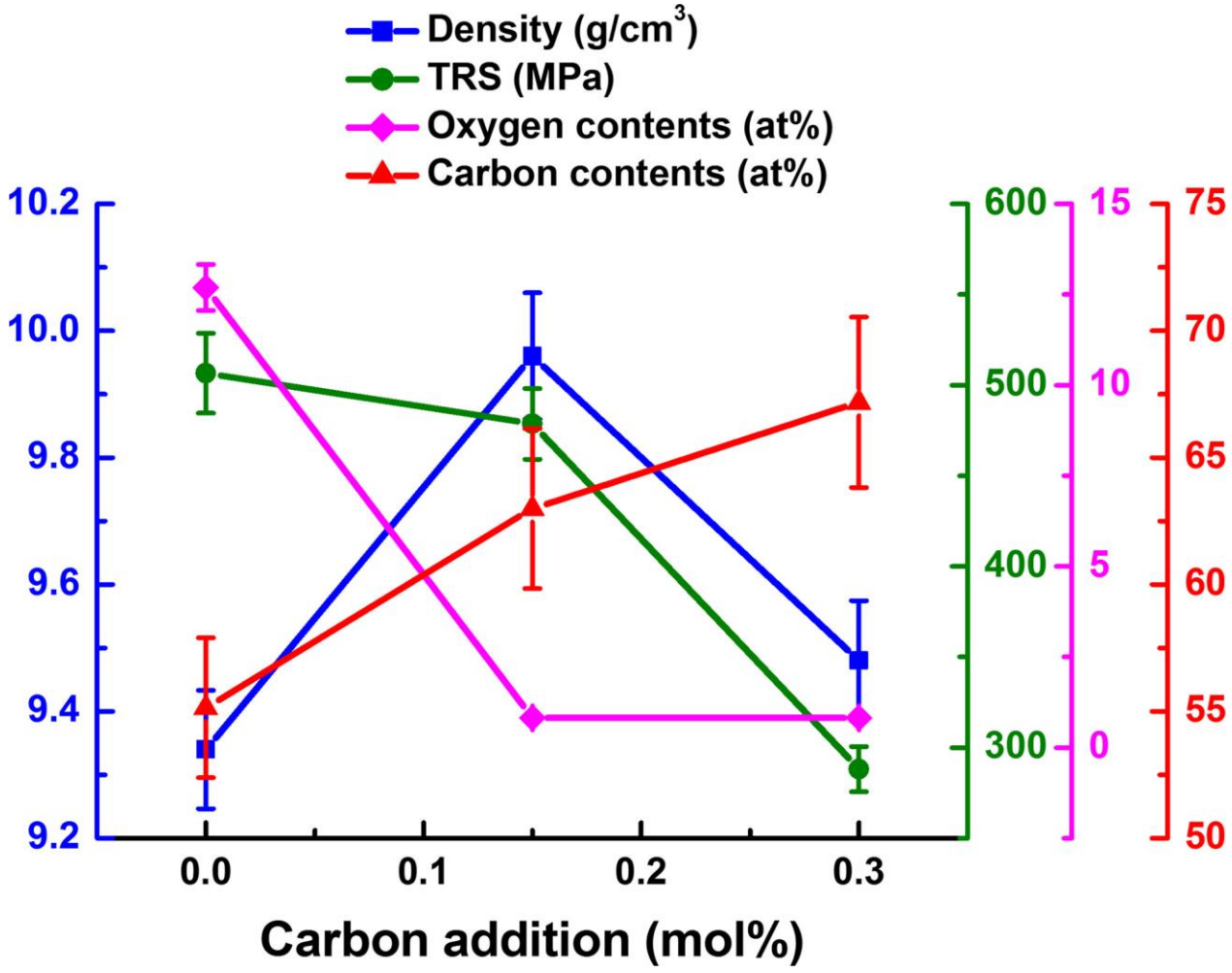

F8 Effect of carbon addition on density, TRS, oxygen contents, and carbon contents of Mo pellets compacted by SPS

There is a high amount of oxygen without carbon addition, as confirmed by SEM (Figure 7A) and EDS (Figure 8). Black arrows indicate the XRD peaks of the MoO2 phase (Figure 7D).56 Due to the addition of the carbon powders, the oxygen contents in the Mo pellets were reduced to almost 1 at.%, as shown in Figure 8. The oxide peaks are removed when 0.15 mol% of carbon was added, and only Mo peaks were shown (ICSD collection code # 76147).57 When carbon additions were increased to 0.3 mol%, the Mo2C peaks (ICSD collection code # 1326)58 were generated. However, as shown in Figures 7A-C, the Mo oxide (red arrows) are still present in the compacted Mo pellets. This means that the oxide phase was reduced with the addition of carbon, yet was not completely removed. The oxygen impurities can still be present in some amounts as a crystalline or amorphous oxide phase, or as a phase dissolved in the Mo lattice, which is below the detection limit of XRD. By reducing the oxide phase at the grain boundaries, the density of Mo samples increased to 9.96 g/cm3 for the 0.15 mol% carbon (Figure 8), which is much higher than that obtained at a higher sintering temperature (maximum apparent density: 9.77 g/cm3 as shown in Figure 5). Due to the low theoretical density of Mo2C (9.18 g/cm3) and a possible remaining

carbon, which did not react with the oxide, the density of the sample with 0.3 mol% carbon addition is lowered compared to that of the sample with 0.15 mol% carbon (Figure 8).

Although the density of the sample increased, and the oxygen content decreased by the carbothermic reduction compared to the sample without carbon addition, the TRS value was reduced, which is apparently due to the increased amount of the remaining carbon which acts as an internal lubricant (Figure 8).26 It should be noted that the carbon content detected by EDS can be induced from not only the remaining carbon powders but also from the carbon deposition during SEM.59 Therefore, the real carbon content of the Mo specimen can be lower than what is shown in Figure 8.

4.5 Surface cleaning of oxidized Mo nanopowders during SPS

A holding stage at 800°C was used, after which the temperature was increased to a maximum of 1200°C or 1700°C. As shown in Figure 9 and Table 2, the oxygen amount in the samples was reduced after holding at 800°C, but not as dramatic as in the carbothermal reduction case (Section 4.5). The density and TRS with the holding stage at 800°C are of higher values than those of Mo pellets processed without the holding stage (Table 2), which can be explained by the reduction in oxygen. The samples sintered at 1700°C with the holding stage at 800°C showed high density (9.94 g/cm3) but large average grain size (73.95 μm). Compared with the samples obtained by the carbothermic reduction with 0.15 mol% carbon, the samples sintered at 1700°C with the holding stage at 800°C have a higher TRS even despite their larger grain size due to the absence of carbon (Figure 8 and Table 2).

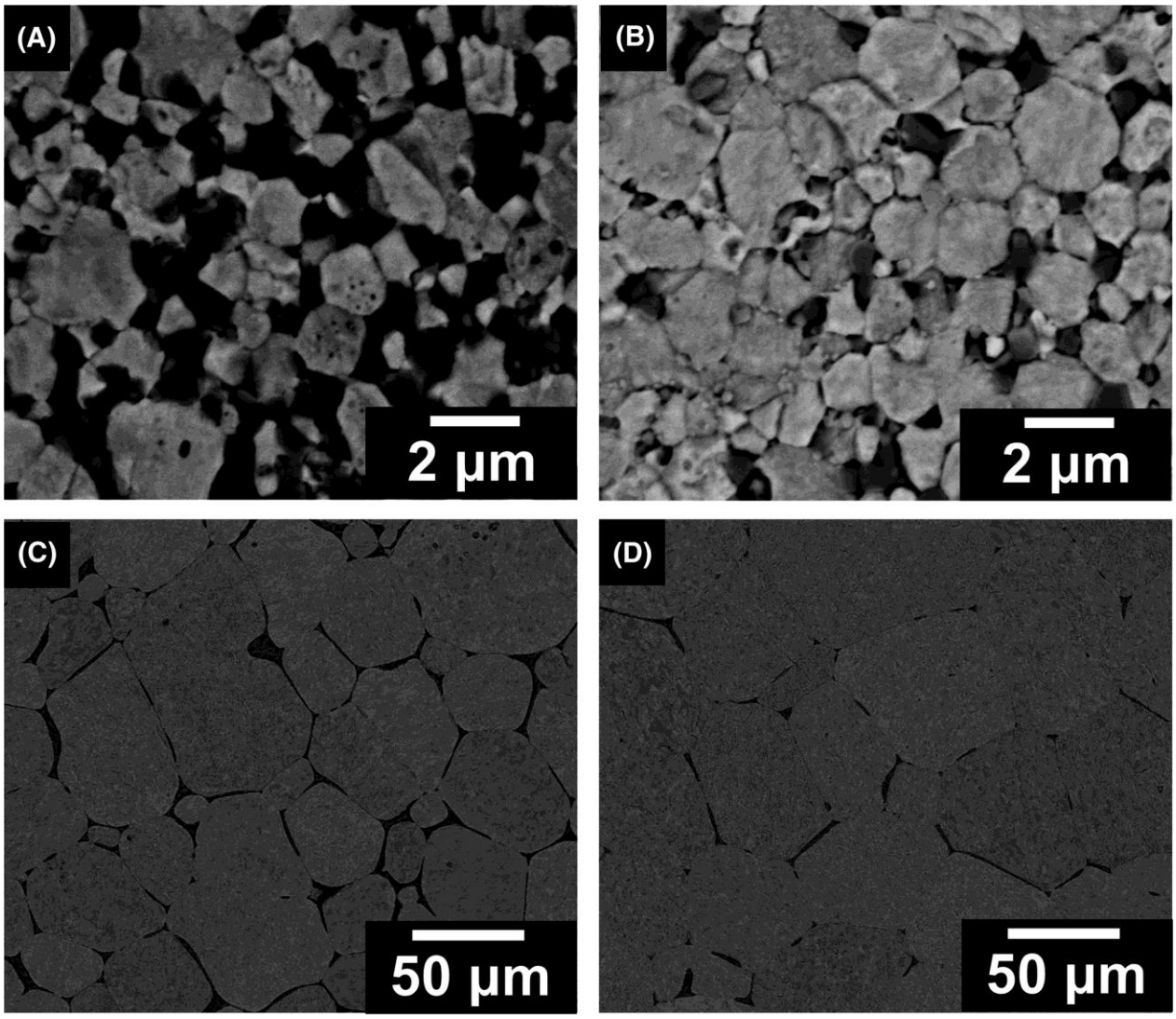

F9 SEM phase images of SPSed Mo pellets without (A and C) and with (B and D) soaking stage at 800°C with the final sintering temperatures of 1200°C (A and B) and 1700°C (C and D)

Table 2. Properties of sintered samples with or without holding stage at 800°C

Sintering temperature (°C)	Holding at 800°C	Oxygen contents (at.%)	Density (g/cm^3)	Grain size (µm)	TRS (MPa)
1200	X	12.6	9.30	1.61	753.31
1200	O	10.3	9.66	1.74	859.99

Sintering temperature (°C)	Holding at 800°C	Oxygen contents (at.%)	Density (g/cm³)	Grain size (µm)	TRS (MPa)
1700	X	6.8	9.61	54.75	671.71
1700	O	4.5	9.94	73.95	711.67

5 CONCLUSIONS

In conclusion, the study of the sintering behavior of Mo nanopowders with the natural oxide layer at the particle surface showed that the density of the processed pellets cannot be increased without removing the oxide phase of the starting powders. The dissociation of the surface oxide accelerates the mass transport, but the remaining oxide surrounding Mo grains still hinders the densification. Also, the TRS is governed by the presence of the oxide phase at the grain boundaries, inducing the embrittlement.

The sintering mechanism of the oxidized Mo nanopowders was obtained by the regression analysis of the experimental data on the regular SPS-based densification, and the SPS multistep pressure dilatometry. The strain rate sensitivity n and activation energy Q values are 4.86 and 324.28 to 384.97 kJ/mol, respectively, indicating the dislocation creep controlled by dislocation climb mechanism of mass transport. Since the grain-boundary diffusion of the Mo atoms is limited by the presence of the melted oxide at the grain boundaries, dislocation climb, which is controlled by lattice diffusion, seems to be a reasonable densification mechanism to assume.

The two in situ oxide reduction methods were employed to remove the oxide during SPS. The carbothermal reduction or the particle surface cleaning by the electric current have been used. Both methods showed a decrease in the oxygen amount and an increase in the final density, but the carbothermal reduction methods showed more promising results in terms of the density and grain size. It was shown that carbon remaining in the samples after the carbothermal reduction process negatively affects the TRS, which lends impetus to analyzing the optimization of the concentration of the carbon amount in the Mo + C powder mixture in future studies.

ACKNOWLEDGMENTS

The support of the U.S. Department of Energy, Materials Sciences Division, under Award No. DE-SC0008581 is gratefully acknowledged.